Journal of Solid State Chemistry 182 (2009) 3254–3261

Contents lists available at ScienceDirect

Journal of Solid State Chemistry

journal homepage: www.elsevier.com/locate/jssc

$K_2Ca_6Si_4O_{15}$—structural and spectroscopical studies on a mixed tetrahedral–octahedral framework

E. Arroyabe, R. Kaindl, D.M. Többens, V. Kahlenberg *

Institute of Mineralogy and Petrography, University of Innsbruck, Innrain 52, A-6020 Innsbruck, Austria

ARTICLE INFO

Article history:
Received 29 June 2009
Received in revised form
4 September 2009
Accepted 13 September 2009
Available online 19 September 2009

Keywords:
Crystal structure
Silicate
Crystal chemistry
Vibrational spectroscopy
Heteropolyhedral framework

ABSTRACT

In the course of an excursion into the system K_2O–CaO–SiO_2, single crystalline material of the previously unknown compound $K_2Ca_6Si_4O_{15}$ has been obtained. Single crystal X-ray diffraction experiments revealed that the new phase is monoclinic (space group $P12/c1$) with the following basic crystallographic data: a=7.3782(8) Å, b=5.5677(5) Å, c=17.2466(17) Å, β=90.005(8)°, Z=2. According to Liebau's nomenclature, the compound can be classified as a mixed anion silicate containing insular $[SiO_4]$-groups as well as $[Si_2O_7]$-dimers in the ratio 2:1, i.e. the crystallochemical formula can be written as $K_2Ca_6[SiO_4]_2[Si_2O_7]$. The silicate anions are linked by K- and Ca-ions distributed among five different non-tetrahedral M-positions and coordinated by six to eight nearest oxygen neighbors. Alternatively, the structure can be described as a heteropolyhedral framework built up by kröhnkite-type $[M(SiO_4)_2O_2]$-chains in which the MO_6 octahedra are corner-linked to bridging SiO_4 tetrahedra. The chains (running parallel to [0 1 0]) are located in 4.6 Å wide layers parallel to (1 0 0). Neighboring sheets are shifted relative to each other by an amount of $+\delta$ or $-\delta$ along [0 0 1]. In the derived two layer …ABABAB… stacking sequence, chains belonging to adjacent sheets are linked by corner sharing of common oxygen atoms. The resulting network contains tunnels in which the more irregularly coordinated K- and Ca-ions are incorporated for charge compensation. A comparison between the present compound and structurally related mixed tetrahedral–octahedral frameworks is given. The characterization has been completed by Raman and FTIR-spectroscopy. An allocation of the bands to certain vibrational species has been aided by density functional theory (DFT) calculations.

1. Introduction

Up to now, the only comprehensive investigation on the system K_2O–CaO–SiO_2 dates back to 1930. In their studies, Morey et al. [1,2] explored the melting relations in the more SiO_2-rich part of the ternary system and reported the existence of the following seven potassium-calcium silicates: $K_2Ca_2Si_9O_{21}$, $K_8CaSi_{10}O_{25}$, $K_4CaSi_6O_{15}$, $K_2Ca_2Si_6O_{15}$, $K_2Ca_3Si_6O_{16}$, $K_4CaSi_3O_9$ and K_2CaSiO_4. Optical features of the crystals served to establish hypotheses concerning the crystal systems, i.e. neither powder/single-crystal diffraction nor spectroscopic data have been collected. Gunawardane and Glasser [3] confirmed the existence of $K_4CaSi_3O_9$ and $K_8CaSi_{10}O_{25}$, respectively, and reported indexed powder diffraction patterns. Powder diffraction data for K_2CaSiO_4 have been published, for example, by Berezhnoi et al. [4]. On the other hand, there are also indications that the list of phases given above is not complete. In the course of investigations on the incorporation of potassium into cement clinker phases [5,6], a $K_2Ca_{23}Si_{12}O_{48}$ compound was reported, probably representing a solid solution of K_2O in α'-Ca_2SiO_4. Akiyama et al. [7] noted the existence of $K_2Ca_2Si_2O_7$, which is claimed to be the main phase in fertilizers obtained from the reaction between potassium carbonate and iron- or steelmaking slags. Furthermore, a potassium calcium silicate with probable composition $K_2Ca_6Si_4O_{15}$ was mentioned [8].

However, these studies listed in the last paragraph are of limited information content since they were restricted, if at all, to the presentation of basic crystallographic data. By now, only the crystal structures of $K_{9.6}Ca_{1.2}Si_{12}O_{30}$ (or $K_8CaSi_{10}O_{25}$) [9] and $K_4CaSi_3O_9$ [10] have been solved from powder diffraction data in our laboratory.

All in all, a detailed inspection of the compound formation, the sub-solidus phase relationships and, consequently, the crystal structures is still missing. This is even more surprising, since the ternary system K_2O–CaO–SiO_2 is definitely of importance for several technologically interesting processes and materials, for example, blast furnace linings [11], combustion ashes [12,13], potassium silicate fertilizers [7,14], and coatings for metals/alloys for biomedical applications [15].

The present paper is a part of an ongoing study on the phase relationships of the K_2O–CaO–SiO_2 system and reports a

* Corresponding author. Institut für Mineralogie und Petrographie, Leopold-Franzens-Universität Innsbruck, Innrain 52, A-6020 Innsbruck.
Fax: +43 512 507 2926.
E-mail address: Volker.Kahlenberg@uibk.ac.at (V. Kahlenberg).

0022-4596/$ - see front matter © 2009 Elsevier Inc. All rights reserved.
doi:10.1016/j.jssc.2009.09.013

structural characterization of $K_2Ca_6Si_4O_{15}$. Furthermore, a detailed structural comparison with other related materials is presented.

2. Experimental details

2.1. Sample preparation and chemical analysis

Single crystals were obtained from a synthesis aiming to produce polycrystalline K_2CaSiO_4. Therefore, a stochiometric mixture of dried K_2CO_3 (AlfaAesar, puratronic), $CaCO_3$ (AlfaAesar, 99.995%) and SiO_2 (AlfaAesar, 99.995%) was carefully homogenized in an agate mortar under ethanol, pressed into pellets, transferred into a platinum crucible and finally heated in a chamber furnace from room-temperature to 800 °C within 24 h, in order to decarbonate the specimen. Subsequently, the sample was pulverized, re-pressed, fired for 7 days at 1000 °C and finally quenched in air. After a first inspection, the run-product turned out to be partially molten. It consisted mainly of colorless, transparent-birefringent crystals with slightly undulous extinction. This result was surprising, since it is in obvious contradiction to the phase diagram given by Morey et al. [1], where K_2CaSiO_4 is reported to melt congruently at about 1600 °C. The total yield of crystalline solids was not greater than 60–70 vol%.

The chemical composition of a single crystal was analyzed with a JEOL JXA 8100 electron microprobe using the wavelength-dispersive analytical mode with 15 kV acceleration voltage and 10 nA beam current. Orthoclase, diopside and quartz were selected as standards for K, Ca and Si, respectively, with measurement times of 20 s on peaks and 10 s on backgrounds of the X-ray lines. The obtained ratio of 1.00(11):1.98(13):2.77(18) for K:Si:Ca resulted in a chemical formula K2.07(68)Ca5.75(38)-Si4.11(37)O15 (normalized on 15 oxygen atoms) or $K_2Ca_6Si_4O_{15}$.

Table 1
Data collection and refinement parameters for $K_2Ca_6Si_4O_{15}$.

Crystal data	
Unit cell dimensions	a=7.3782(8) Å b=5.5677(5) Å c=17.2466(17) Å β=90.005(8)°
Volume	708.48(12) Å^3
Space Group	$P2/c$
Z	2
Chemical formula	$K_2Ca_6Si_4O_{15}$
Crystal system	Monoclinic
Density (calculated)	3.146 g cm^{-3}
Absorption coefficient	3.265 mm^{-1}
Intensity measurements	
Crystal shape	Plate
Crystal size	0.105 × 0.09 × 0.015 mm
Diffractometer	STOE-IPDS-II
Monochromator	Graphite
Radiation	MoKα, λ=0.71073 Å
Temperature	25 °C
Generator settings	50 kV, 40 mA
Index ranges	$-10 \le h \le 10$, $-7 \le k \le 7$, $-23 \le l \le 22$
No. of refelections collected	6354
No. of unique reflections	1883
No. of observed reflections ($I > 4\sigma(I)$)	1717
R(int) after absorption correction	0.0247
Refinement parameters	
No. of parameters	124
No. of restraints	0
Final R indices [$I > 2$sigma(I)]	$R1$=0.0274, w$R2$=0.0605
Final R indices (all data)	$R1$=0.0326, w$R2$=0.0621
Goodness-of-fit on F^2	1.177
Largest diff. peak and hole	0.505 and −0.349 e Å^{-3}

2.2. X-ray data collection and structure analysis

In order to investigate the obtained product in more detail, a small platy crystal (0.105 × 0.09 × 0.015 mm in size) of comparatively good optical quality was selected for a single crystal X-ray diffraction study. The data were collected at ambient temperature on a STOE-IPDS-II single crystal diffractometer. The X-Area software package [16] was used for data collection, integration and reduction. Although the metric symmetry of the unit cell was orthorhombic, merging of the symmetry equivalent reflections in Laue group mmm and the possible subgroups clearly showed, that the crystal belongs to the monoclinic crystal system ($R_{int.}(mmm)$=0.384; $R_{int.}(12/m1)$=0.025). Furthermore, the test procedures implemented in the program TWIN3.0 [17,18] indicated the absence of twinning by pseudo-merohedry which is likely to occur in cases of monoclinic symmetry when $\beta \approx 90°$. The analysis of the systematic absences resulted in two possible space groups: $P1c1$ and $P12/c1$, respectively. Intensity statistics ($\langle |E^2-1| \rangle$) strongly suggested, that the compound is centrosymmetric. The structure was solved completely in space group $P12/c1$ by dint of direct methods using the SIR2004 suite [19]. Due to the resulting linear absorption coefficient of 3.265 mm^{-1} for

Table 2
Atomic coordinates and equivalent isotropic displacement parameters [Å^2] for $K_2Ca_6Si_4O_{15}$.

	Wyckoff-site	x	y	z	U(eq)	Occupancy
M(1)	4g	0.2460(1)	0.2400(1)	0.0911(1)	0.010(1)	1.0 Ca
M(2)	2f	0.5000	0.1612(1)	0.2500	0.012(1)	0.91 Ca/0.09 K
M(3)	2e	0	0.2036(1)	0.2500	0.016(1)	0.76 Ca/0.24 K
M(4)	4g	0.5096(1)	0.7339(1)	0.0827(1)	0.014(1)	0.90 Ca/0.10 K
M(5)	4g	0.9719(1)	0.7460(1)	0.0834(1)	0.015(1)	0.26 Ca/0.74 K
Si(1)	4g	0.7349(1)	0.2483(1)	0.0639(1)	0.010(1)	
Si(2)	4g	0.2238(1)	−0.2876(1)	0.2366(1)	0.009(1)	
O(1)	4g	0.9299(2)	0.2488(3)	0.1088(1)	0.020(1)	
O(2)	4g	0.2755(2)	0.5297(3)	−0.0005(1)	0.017(1)	
O(3)	4g	0.2914(2)	−0.0026(3)	−0.0132(1)	0.018(1)	
O(4)	4g	0.2548(2)	0.4349(3)	0.2130(1)	0.019(1)	
O(5)	4g	0.2699(2)	−0.1047(3)	0.1656(1)	0.020(1)	
O(6)	2e	0	−0.2552(5)	0.2500	0.023(1)	
O(7)	4g	0.3187(2)	−0.1871(3)	0.3126(1)	0.020(1)	
O(8)	4g	0.5566(2)	0.2874(3)	0.1182(1)	0.015(1)	

In contrast to the M(1)-position, which is exclusively occupied by Ca, the sites M(2)-M(5) exhibit mixed Ca/K populations (see text). U(eq) is defined as one third of the trace of the orthogonalized U_{ij} tensor.

MoKα-radiation a semi-empirical absorption correction [20] was applied. Consecutive least-squares refinement cycles were carried out with the program SHELX97 [21]. An initially introduced Larson-type extinction correction was later discarded, since the refined extinction coefficient was equal to zero within two standard uncertainties. The final computations using anisotropic displacement parameters for all atoms resulted in a residual of $R1=0.0274$ for 124 parameters for all reflections with $I>2\sigma(I)$ (see Table 1). Refined atomic coordinates, anisotropic displacement parameters as well as selected interatomic distances and angles are given in Tables 2–4, respectively. Figures showing structural details were prepared using the program ATOMS5.1 [22].

Table 3
Anisotropic displacement parameters [Å^2] for $K_2Ca_6Si_4O_{15}$.

	U_{11}	U_{22}	U_{33}	U_{23}	U_{13}	U_{12}
M(1)	0.010(1)	0.010(1)	0.009(1)	0.000(1)	0.001(1)	0.000(1)
M(2)	0.012(1)	0.014(1)	0.010(1)	0	0.000(1)	0
M(3)	0.014(1)	0.016(1)	0.017(1)	0	0.004(1)	0
M(4)	0.012(1)	0.016(1)	0.013(1)	−0.002(1)	0.000(1)	0.001(1)
M(5)	0.015(1)	0.015(1)	0.016(1)	−0.001(1)	−0.002(1)	0.000(1)
Si(1)	0.009(1)	0.010(1)	0.010(1)	0.000(1)	0.001(1)	−0.001(1)
Si(2)	0.008(1)	0.010(1)	0.009(1)	0.000(1)	0.001(1)	0.000(1)
O(1)	0.011(1)	0.023(1)	0.027(1)	0.002(1)	−0.003(1)	−0.001(1)
O(2)	0.021(1)	0.013(1)	0.016(1)	0.004(1)	−0.001(1)	−0.001(1)
O(3)	0.027(1)	0.013(1)	0.014(1)	−0.003(1)	0.002(1)	−0.001(1)
O(4)	0.022(1)	0.016(1)	0.018(1)	−0.006(1)	−0.004(1)	0.004(1)
O(5)	0.017(1)	0.022(1)	0.021(1)	0.010(1)	0.004(1)	0.001(1)
O(6)	0.009(1)	0.038(1)	0.021(1)	0	0.003(1)	0
O(7)	0.022(1)	0.020(1)	0.018(1)	−0.007(1)	−0.006(1)	0.002(1)
O(8)	0.011(1)	0.023(1)	0.012(1)	0.001(1)	0.002(1)	0.001(1)

The anisotropic displacement factor exponent takes the form: $-2\pi^2[h^2a^{*2}U_{11}+\ldots+2\,h\,k\,a^*\,b^*\,U_{12}]$.

Table 4
Selected bond lengths [Å] (up to 3.05 Å) and angles [°].

M(1)–O(2)	2.2678(15)	*M*(3)–O(4)	2.3670(17) × 2
M(1)–O(3)	2.2738(16)	*M*(3)–O(1)	2.5021(18) × 2
M(1)–O(5)	2.3167(16)	*M*(3)–O(6)	2.5544(28)
M(1)–O(1)	2.3525(16)	*M*(3)–O(5)	3.0045(17) × 2
M(1)–O(8)	2.3538(15)	*M*(3)–O(6)	3.0133(28)
M(1)–O(4)	2.3663(16)		
		M(4)–O(7)	2.2495(16)
		M(4)–O(3)	2.4158(16)
		M(4)–O(5)	2.4456(16)
M(2)–O(8)	2.4156(15) × 2	*M*(4)–O(2)	2.5166(16)
M(2)–O(4)	2.4501(16) × 2	*M*(4)–O(8)	2.5834(16)
M(2)–O(7)	2.5911(18) × 2	*M*(4)–O(2)	2.5845(16)
M(2)–O(5)	2.6818(17) × 2	*M*(4)–O(3)	2.7346(16)
M(5)–O(3)	2.6986(17)	Si(1)–O(8)	1.6291(15)
M(5)–O(5)	2.7447(17)	Si(1)–O(1)	1.6342(16)
M(5)–O(2)	2.7809(16)	Si(1)–O(3)	1.6354(16)
M(5)–O(1)	2.8198(17)	Si(1)–O(2)	1.6520(16)
M(5)–O(7)	2.8214(18)		
M(5)–O(1)	2.8505(17)	Si(2)–O(7)	1.5878(16)
M(5)–O(6)	2.8809(5)	Si(2)–O(4)	1.6139(16)
M(5)–O(2)	2.9258(17)	Si(2)–O(5)	1.6279(16)
		Si(2)–O(6)	1.6773(6)
O(8)–Si(1)–O(2)	104.08(8)	O(5)–Si(2)–O(6)	104.01(9)
O(3)–Si(1)–O(2)	105.43(8)	O(4)–Si(2)–O(6)	106.10(11)
O(8)–Si(1)–O(3)	108.88(9)	O(7)–Si(2)–O(6)	106.40(8)
O(1)–Si(1)–O(2)	110.67(8)	O(7)–Si(2)–O(5)	107.92(9)
O(1)–Si(1)–O(3)	111.05(9)	O(4)–Si(2)–O(5)	112.32(9)
O(8)–Si(1)–O(1)	116.01(9)	O(7)–Si(2)–O(4)	118.89(9)
Mean	109.35	Mean	109.27
Si(2)–O(6)–Si(2)	167.66(19)		

2.3. Raman spectroscopy

Confocal Raman spectra of a single crystal were obtained with a HORIBA JOBIN YVON LabRam-HR 800 Raman micro-spectrometer. The sample was excited using the 514.5 nm emission line of a 30 mW Ar^+-laser and an OLYMPUS 100× objective (N.A.=0.9). Size and power of the laser spot on the surface were approximately 1 μm and 2 mW. The spectral resolution, determined by measuring the Rayleigh line, was about 2 cm^{-1}. The dispersed light was collected by a 1024 × 256 open electrode CCD detector. Confocal pinhole was set to 1000 μm. Spectra were recorded unpolarized. The data were corrected assuming second-order polynomial background and fitted to Gauss-Lorentz functions. Accuracy of Raman line shifts, calibrated by regular measuring of the Rayleigh line, was in the order of 0.5 cm^{-1}.

2.4. FTIR-spectroscopy

FTIR absorption spectra of thin aggregates of the polycrystalline material, which was placed on a ZnSe plate, were recorded in transmission with a Bruker Vertex 70 FTIR spectrometer attached to a Hyperion 3000 microscope in a spectral range from 550–4000 cm^{-1}. The spectra were corrected assuming second-order polynomial background and fitted to Gauss-Lorentz functions.

3. Description of the crystal structure

According to Liebau's classification of silicates [23], the crystal structure of $K_2Ca_6Si_4O_{15}$ belongs to the group of mixed-anion silicates containing isolated [SiO_4]-tetrahedra as well as [Si_2O_7]-dimers in the ratio of 2:1. Therefore, the crystallochemical formula of the compound can be written as $K_2Ca_6[SiO_4]_2[Si_2O_7]$. As shown in Fig. 1, the tetrahedral units are arranged in layers perpendicular to [0 0 1]. Charge compensation within the structure is accomplished by K^+- and Ca^{2+}-cations, which are distributed among a total of five crystallographically different non-tetrahedral *M*-positions.

Concerning the spread of the Si–O bond distances, the two tetrahedral building units behave quite differently. Whereas the

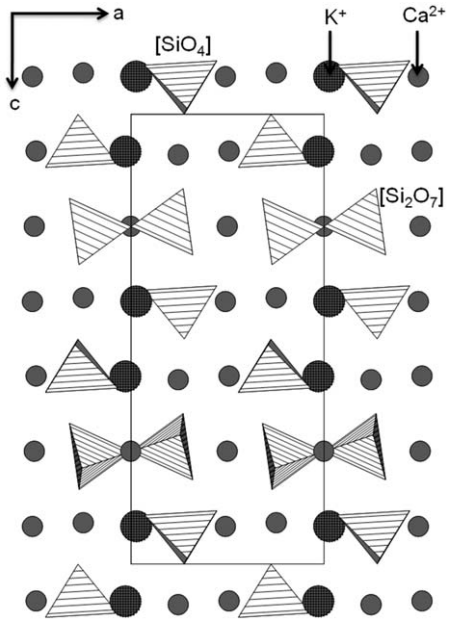

Fig. 1. Projection of the whole crystal structure of $K_2Ca_6[SiO_4]_2[Si_2O_7]$ parallel to [0 1 0].

scatter within the insular tetrahedron around Si(1) is not very pronounced (1.629–1.652 Å), the corresponding values for the dimeric unit (formed by two symmetrically equivalent [Si(2)O_4]-tetrahedra) range between 1.588–1.677 Å, respectively. However, the observed variation follows the expected trend for [Si_2O_7]-groups having one bridging and three terminal atoms: the distances between the silicon atoms and the terminal oxygens (O(4), O(5), O(7)) are considerably shorter (average: 1.610 Å) than the corresponding bond length to the bridging oxygen O(6) (1.677 Å). The shortening of the Si–O_{term} bond lengths (by an average of 0.067 Å) results from the stronger attraction between O and Si than between O and the other cations in the structure. The distortion is also reflected in the O–Si–O angles ranging from 104.08° to 116.01° (for Si(1)) and from 104.01° to 118.89° (for Si(2)), respectively. Nevertheless, the mean ⟨O–Si–O⟩ angles are close to the ideal value for an undistorted tetrahedron. The tetrahedral distortion can be expressed numerically via the quadratic elongation and the angle variance [24]. The values of these parameters are λ=1.004 and σ^2=18.50 for Si(1) as well as λ=1.007 and σ^2=29.83 for Si(2), respectively. The Si–O–Si angle has a value of 167.66°. Since O(6), the bridging oxygen of the [$Si(2)_2O_7$]-unit, is located on a special position ($2_{[0\,1\,0]}$), only two symmetrically independent angles of torsion can be distinguished within the dimer: <[O(7)–Si(2)–Si(2)–O(5)]=19.32(9)° (=<[O(5)–Si(2)–Si(2)–O(7)]), and <[O(4)–Si(2)–Si(2)–O(4)]=10.55(5)°, respectively, i.e. the conformation can be considered as fully eclipsed (Fig. 2).

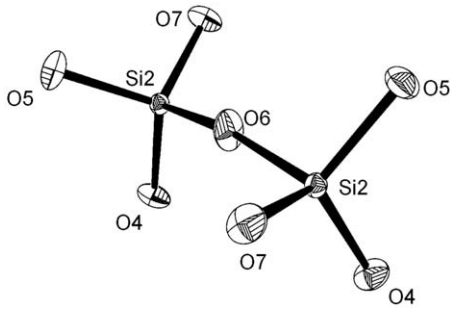

Fig. 2. Side view of a single [Si_2O_7]-group in $K_2Ca_6[SiO_4]_2[Si_2O_7]$. Thermal displacement ellipsoids are drawn at the 50% probability level.

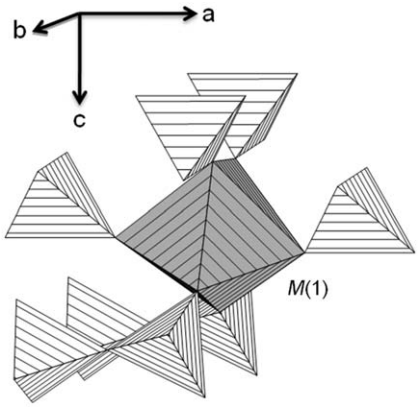

Fig. 3. Side view of the connectivity of a single $M(1)O_6$-octahedron and the surrounding tetrahedra.

The non-tetrahedral $M(1)$ position is coordinated by six nearest oxygen neighbors in form of a distorted octahedron. As shown in Fig. 3, each octahedron shares common corners with four adjacent insular tetrahedra and two different [Si_2O_7]-dimers. The coordination spheres of the remaining M-sites are much more irregular involving 7–8 oxygen ligands.

Because K^+ and Ca^{2+} are isoelectronic cations, refinements of the site populations based on the X-ray diffraction data cannot be used to reveal evidence for K↔Ca substitutions on the M-sites. Since typical Ca–O and K–O distances average at about 2.33 and 2.76 Å [25], $M(1)$ should correspond to a pure Ca-site (⟨$M(1)$–O⟩=2.322 Å), whereas $M(5)$ should be dominated by potassium (⟨$M(5)$–O⟩=2.815 Å). For the $M(2)$, $M(3)$ and $M(4)$ positions mixed K/Ca populations can be expected. A quantitative determination of the site occupancies for the five M-sites was performed with the Program OccQP [26] using quadratic programming tools

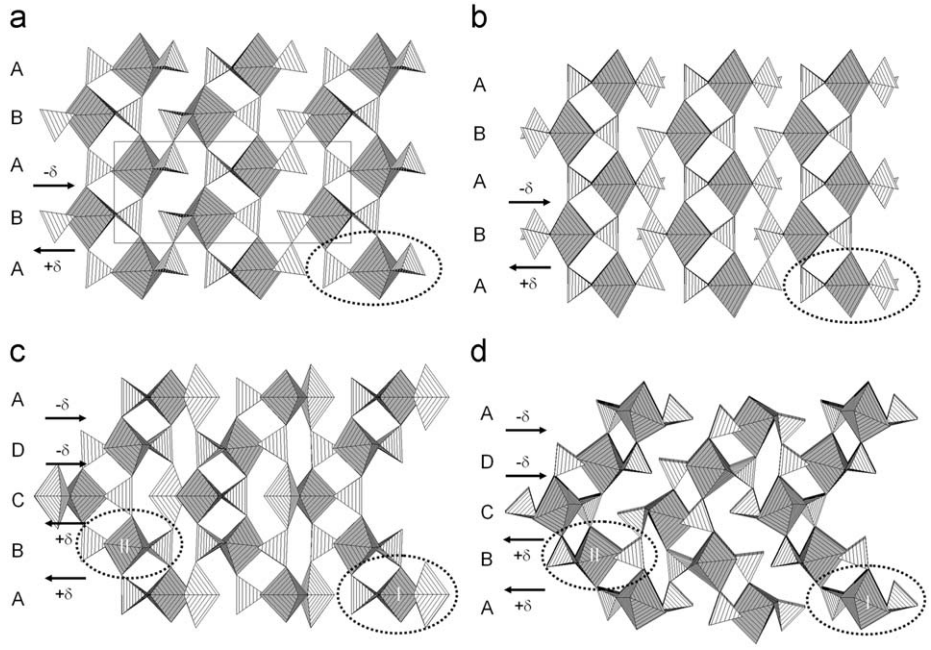

Fig. 4. Projections of the mixed tetrahedral–octahedral frameworks of (a) $K_2Ca_6[SiO_4]_2[Si_2O_7]$, (b) $Na_2Ba_6[SiO_4]_2[Si_2O_7]$, (c) $Na_2Mg_6[VO_4]_2[V_2O_7]$ and (d) $Na_2Ca_6[SiO_4]_2[Si_2O_7]$. Kröhnkite-type fundamental chains have been encircled.

available in the MATLAB programming environment. The program assigns the substituents to particular sites in order to fit site valences according to the observed chemical analysis (i.e. four K and 12 Ca atoms per unit cell). The resulting cation distributions are as follows: $M(2)$: 91%Ca,9%K; $M(3)$: 76%Ca,24%K; $M(4)$: 90%Ca,10%K and $M(5)$: 26%Ca,74%K. The $M(1)$ position was found to be fully occupied by calcium.

Alternatively, the structure can be described as a mixed tetrahedral–octahedral framework (see Fig. 4a). Within this network, infinite $[M(1)(SiO_4)_2O_2]$-chains running parallel to [0 1 0] can be identified, in which the $M(1)O_6$ octahedra are corner-linked to bridging SiO_4 tetrahedra (see Fig. 5a). They

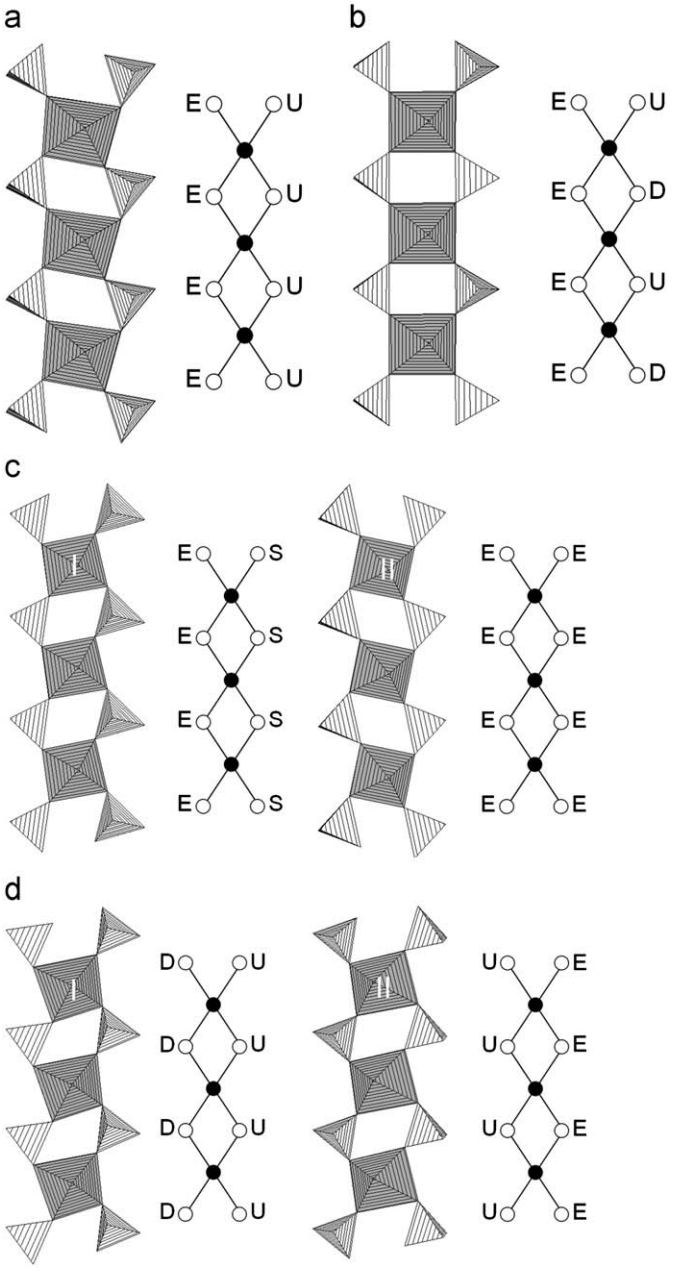

Fig. 5. Projections of single kröhnkite-type chains perpendicular to the plane of the chain for (a) $K_2Ca_6[SiO_4]_2[Si_2O_7]$, (b) $Na_2Ba_6[SiO_4]_2[Si_2O_7]$, (c) $Na_2Mg_6[VO_4]_2[V_2O_7]$ and (d) $Na_2Ca_6[SiO_4]_2[Si_2O_7]$. Black-and-white graphs show the connectivity of the tetrahedra and octahedra (symbolized by white and black circles, respectively). Capital letters indicate the orientation of the tetrahedral units. More details concerning nomenclature are given in the corresponding paragraph in the text.

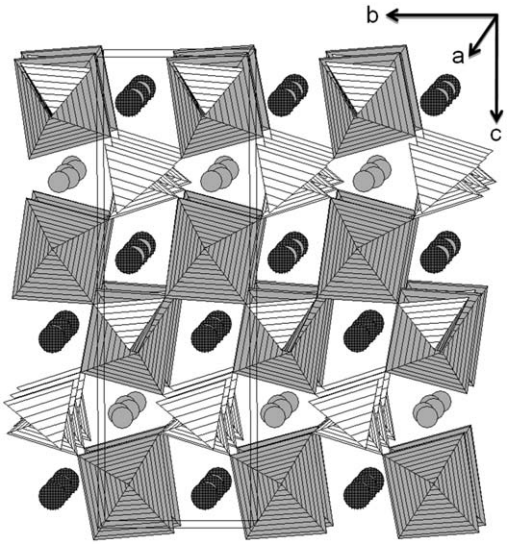

Fig. 6. Side view of the whole heteropolyhedral framework in $K_2Ca_6[SiO_4]_2[Si_2O_7]$. The irregularly coordinated extra-framework cations are shown as spheres.

correspond to a well-known fundamental building unit of structural inorganic chemistry. These so-called "kröhnkite-type" chains (named after the mineral kröhnkite ($Na_2Cu(SO_4)_2 \cdot 2H_2O$)) have been reported to exist in a large number of natural and synthetic compounds. For a recent review the reader is referred to the paper of Kolitsch and Fleck [27] and the references cited therein. A concise graphical representation of the topological structure of the chains is given in Fig. 5a. In this black-and-white sketch the black circles correspond to the octahedral units, whereas the tetrahedra are represented by the white knots. The four thin lines in turn indicate that every octahedron in the chain shares four corners with neighboring $[SiO_4]$-tetrahedra. This type of nodel representation has been developed by Hawthorne [28] and successfully applied to mixed tetrahedral–octahedral chains [29]. Furthermore, the orientation of the tetrahedra relative to the plane of the chain is given by the letters U (for "up"), D (for "down") and E (for "edge", i.e. one of the edges of the tetrahedron is almost perpendicular to the plane of the chain). In the present compound, the chains are located in 4.6 Å wide layers running parallel to (1 0 0). Within a single layer, the chains are arranged in a zig-zag pattern due to displacements of adjacent strings by one half of the translation period along the chain direction. Neighboring sheets in turn are shifted relative to each other by an amount of $+\delta$ or $-\delta$ along [0 0 1]. In the derived two layer …ABABAB… stacking sequence, chains belonging to adjacent sheets are linked by corner sharing of common oxygen atoms (see Fig. 4a). The resulting network contains tunnels in which the more irregularly coordinated K- and Ca-ions are incorporated for charge compensation (Fig. 6).

4. Raman/FTIR spectroscopical results and modeling

The vibrational frequencies have been computed from first principles. Therefore, a fully ordered structure had to be assumed. To preserve maximum agreement with the observed cation distribution (Table 2), potassium was placed on $M(5)$, with calcium occupying $M(1)$–$M(4)$. The computations were performed with the program CRYSTAL 06 [30], using Gaussian basis sets. Basis sets for calcium, silicon, and oxygen were taken from [31], using the values from grossular for Ca, and from andradite for Si and O used therein. The contractions are 86-511G(21), 86-311G(1), 84-11G(1) for Ca, Si, O, respectively. For potassium the 86-511G(3)

Table 5
Experimental and calculated wavenumbers [cm^{-1}] and vibrational types of the Raman-active modes of $K_2Ca_6Si_4O_{15}$.

Exp.	Calc.	Type	Exp.	Calc.	Type
110	112	sb(Ca–O)	532	520	b(Ca–Si–O)
115	119	sb(K–O)	546	551	b(Ca–Si–O)
127	131	s(K–O), sb(K–Ca–Si–O)	556	555	b(Ca–Si–O)
140	137	sb(K–Si)	568	562	b(K–Si–O)
145	–		578	575	b(Ca–Si–O)
154		sb(K–Ca–Si–O)			bo(Ca–Si–O), bo(O–Si–O)
	154		588	589,593	
158	159	b(K–Ca–O)	635	–	–
161	164	sb(K–Ca–O)	667	648	b(O–Si–O)
173	167,172	s(K–O), sb(K–Si)	710	–	–
183		b(K–O), sb(K–Ca–O), sb(K–O)			
	179,181,183		823		
189	186,191	b(K–Ca–O), b(Ca)	825		
199	199,202	s(K–Ca–O), b(O–Ca–O)	846	–	–
206	208	bs(Ca–Si–O)	854	851	s(Si–O)
221		sb(Ca–Si–O), sb(K–Ca–O), b(Ca–K–O)			s(Si–O)
	218,219,221		860	859	
233	230,232	s(Ca–O), sb(K–Ca–O)	866	861	s(Si–O)
241		sb(K–Ca–O), b(Ca), sb(Ca–O)			s(Si–O)
	238,242,248		879	879	
253		b(Ca), s(Ca–O–Ca), b(Ca–O),sb(K–Ca–Si–O), sb(K–Ca–O)			s(Si–O)
	254,255,256,260,264		889	888	
275	274,277	bs(O–Ca–O), s(Ca–Si–O)	895	–	
285	281	sb(Ca–O)	903	906	s(Si–O)
299	290	b(O–Ca–O)	921	915	s(Si–O)
306		sb(Ca–K–Si–O), sb(Ca–K), sb(Ca–Si–O)			s(Si–O)
	304,306,311		925	921	
323	323,327	s(Ca–O), b(Ca–Si–O)	947	937,941,948,952	s(Si–O), s(Ca–Si–O)
331	333	s(Ca–O)	963	964	s(Si–O)
341	343	s((Ca–O)	971	–	
351	351	s(Ca–Si–O)	982	–	
362	–		990	–	
372		sb(K–Ca–O), sb(K–Ca–Si–O), s(K–Ca–O)			
	374,377,385		993	–	
396	399	s(K–Ca–O)	1001	–	
409	403	b(Ca–Si–O)	1010	–	
426	422,423	b(K–Ca–Si–O), b(Ca–Si–O)	1014	–	
437	446	bs(K–Ca–Si–O)	1044	1035	s(Si–O)
482	467,471,490	b(O–Si–O), b(Ca–Si–O)	1072	1072	s(Si–O)
512	510	b(Ca–Si–O)			

Abbreviations: Exp.=experimental, calc.=calculated, s=stretching, b=bending, o=other; in brackets the atoms dominating the specific vibrational mode are given.

basis of [32] was adopted. Attempts to further optimize the most diffuse shells did not result in a significant improvement. The Dirac-Slater (LDA) exchange functional [33] in combination with the Vosko-Wilk-Nusair (VWN) correlation functional [34] was employed. This simple local density approximation was found to give results superior to more sophisticated gradient corrected or hybrid models. A Pack-Monkhorst k net with $4\times4\times4$ points in the Brillouin zone was used. Modified Broyden damping [35] was applied. The unit cell resulting from this model is uniformly 1% smaller than the experimental unit cell, with negligible anisotropy of the deviation. The Raman shifts and IR absorption frequencies were calculated from the fully relaxed structure, agree with the experimental spectrum with a maximum deviation of $30\,cm^{-1}$. For $K_2Ca_4Si_8O_{21}$, where almost no disorder of K and Ca on the non-tetrahedral *M*-sites was observed, the same model gave a much better agreement with maximum deviations of $15\,cm^{-1}$ (to be published). It is therefore reasonable to assume, that the deviations are a result of the occupational disorder of the real structure.

The computation yielded the following irreducible representation of $K_2Ca_6Si_4O_{15}$ (point group $2/m$ or C_{2h}):

$$\Gamma_{\mathrm{Vib}} = 39A_g + 39A_u + 42B_g + 42B_u$$

A_g and B_g modes are Raman-active, A_u and B_u modes are IR-active. This means, that theoretically a total number of 81 modes should be present in the Raman spectrum. Experimentally, we observed only 67 Raman and 12 IR-bands. This can be explained by the partly very low frequency differences between *A* and *B* modes, exceeding the resolution of the spectrometer.

Table 6
Experimental and calculated wavenumbers [cm^{-1}] and vibrational types of the IR-active modes of $K_2Ca_6Si_4O_{15}$.

Exp.	Calc.	Type
561	567	b(Ca–Si–O)
571	570	b(O–Si–O)
588	586	b(O–Si–O)
	–	–
	–	b(O–Si–O)
668	654	b(O–Si–O)
	–	–
	–	–
	–	–
836	846	s(Si–O)
862	860,863,878,880	s(Si–O)
908	923,925,933,935	s(Si–O)
939	944,949	s(Si–O),s(Ca–Si–O)
979	961	s(Si–O)
	993	s(O–Si–O)
1027	1038	s(Si–O)
1051	1046	s(Si–O)
1116	–	–

Comparisons of the experimentally determined and calculated mode frequencies are given in Tables 5 and 6.

The density of Raman and IR-active modes in the spectrum of $K_2Ca_4Si_8O_{21}$ is high, both for the observed and the calculated spectrum (see Figs. 7 and 8, respectively). For a number of isolated modes the assignment of observed and calculated frequencies is unequivocal. From these the maximum deviation between experimental and calculated spectrum can be estimated to be about 30 cm^{-1}. For most of the signals therefore various modes can be assigned. This level of uncertainty should be kept in mind when interpreting the assignments given in Tables 5 and 6.

Groupwise, all modes in the upper range (850–1070 cm^{-1}) are Si–O stretching modes. O–Si–O bending modes are found predominately in the range 460–660 cm^{-1}, but extend down to 400 cm^{-1}. O–Ca–O bending modes appear in the range 350–450 cm^{-1}, Ca–O stretching modes at 230–440 cm^{-1}. Modes dominated by potassium appear only below 230 cm^{-1}. IR-active modes below 550 cm^{-1} could not be experimentally determined and are therefore not discussed.

Of particular interest are the strong peaks dominating the spectrum. The signal a 667 cm^{-1} in the Raman spectrum is a O–Si(2)–O bending mode of A_g symmetry, followed by a spectral gap of about 150 cm^{-1}. The strongest mode at 823 cm^{-1} is presumably a Si–O stretching mode. The calculations confirm a gap between O–Si–O bending (648) and Si–O stretching modes (851), albeit the gap is larger (about 200 cm^{-1}). In the IR-spectrum the experimentally determined gap between 668 and 836 cm^{-1} coincides quite well with the calculations (654 and 846 cm^{-1}). The doublet of Raman-active modes at 854 and 860 cm^{-1} consists of two Si(1)–O stretching modes, of A_g and B_g symmetry. A broad band at 862 cm^{-1} is also observed in the IR-spectrum and can be correlated with in total four calculated Si(1)–O stretching modes (860, 862, 878, 880 cm^{-1}) of A_u and B_u symmetry. It is interesting to note that the agreement between the observed and the calculated Raman shifts and IR absorption maxima is much better for those modes dominated by Si(1), while comparably high deviations are observed for those modes dominated by Si(2). The cause for this might be the cation disorder. The cation sites with the highest degree of disorder are *M*(3) and *M*(5). These sites lie in a common plane with the center of the $Si(2)_2O_7$ dimers. The $Si(1)O_4$ tetrahedra lie above these plane, and contribute much less to the coordination spheres of these cations. Consequently, the strong distortions of the $Si(2)_2O_7$ dimers also distort the coordination spheres of *M*(3) and *M*(5). It is reasonable to assume that a wrong occupation of these sites in the model would affect these modes the most.

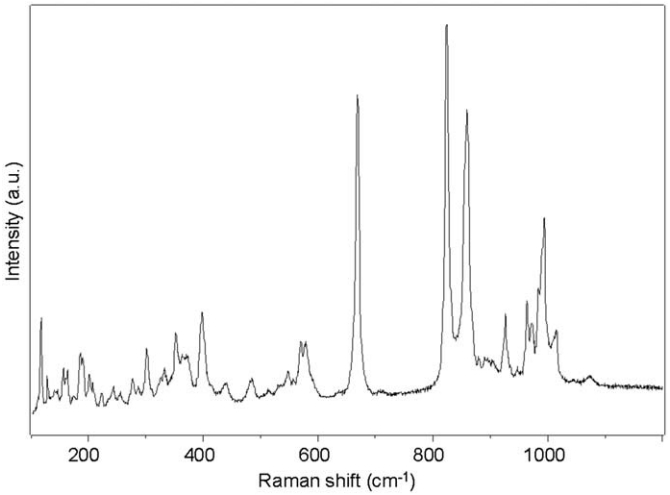

Fig. 7. Raman spectrum of polycrystalline $K_2Ca_6[SiO_4]_2[Si_2O_7]$.

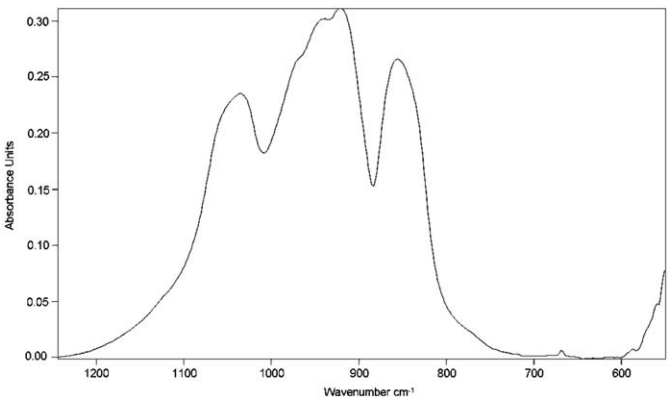

Fig. 8. FTIR-spectrum of polycrystalline $K_2Ca_6[SiO_4]_2[Si_2O_7]$.

5. Discussion and comparison with related structures

The number of minerals belonging to the group of mixed-anion silicates containing insular tetrahedra and diortho-groups is rather limited. Examples include well-known rock-forming minerals such as epidote $Ca_2(Fe,Al)_3[SiO_4][Si_2O_7]O(OH)$ [23], zoisite $Ca_2Al_3[SiO_4][Si_2O_7]O(OH)$ [23], pumpellyite $Ca_2MgAl_2[SiO_4][Si_2O_7](OH)_2{}^*H_2O$ [23] or vesuvianite $Ca_{10}(Fe,Mg)_2Al_4[SiO_4]_5[Si_2O_7]_2(OH)_4$ [23], but also more exotic species such harstigite $MnCa_6Be_4[SiO_4]_2[Si_2O_7]_2(OH)_2$ [36] or rustumite $Ca_{10}[SiO_4][Si_2O_7]_2Cl_2(OH)_2$ [37]. Most of these compounds contain single and double tetrahedra in the ratio 1:1. To our best knowledge, so far no silicate mineral with a ratio of 2:1 has been described. However, a search in the recent volume of the Inorganic Crystal Structure Database (Version 1.4.6) revealed the following synthetic compounds to have the same 2:1 ratio as $K_2Ca_6[SiO_4]_2[Si_2O_7]$: $Na_2Ca_6[SiO_4]_2[Si_2O_7]$ [38], $Na_2Ba_6[SiO_4]_2[Si_2O_7]$ [39], $Na_2Mg_6[VO_4]_2[V_2O_7]$ [40] and $Li_2HBa_6[SiO_4]_2[Si_2O_7]Cl$ [41]. Furthermore, three compounds homoetypic with $Na_2Ca_6[SiO_4]_2[Si_2O_7]$ have been verified only recently [42]: $Na_4Sr_2Y_2[SiO_4]_2[Si_2O_7]$, $Na_4Sr_2In_2[SiO_4]_2[Si_2O_7]$ and $Na_4Sr_2Sc_2[SiO_4]_2[Si_2O_7]$, respectively. Compared to the material under investigation the first three compounds were of special interest since their chemical formulas pointed to a possible closer structural relationship. A more detailed analysis of crystal structures corroborated this hypothesis. The phases can be also classified as tetrahedral–octahedral frameworks based on layer-like arrangements of the same kröhnkite-type chains that have been used as a fundamental building block for the description of the corresponding K–Ca-phase (see above). Especially the Na–Ba-phase exhibits considerable similarities with the K–Ca-compound. In both materials a …ABABAB… stacking of the layers is observed. Furthermore, the sequence of relative shifts of neighboring layers perpendicular to the chain direction is identical: $\ldots+\delta,-\delta,+\delta,-\delta,\ldots$ (see Fig. 4a and b). Apart from distortions induced by unlike rotations of the polyhedra about the bridging oxygens, further important differences can be attributed to the orientations of the tetrahedra within the chains. Whereas in the K–Ca-silicate adjacent layers contain chains with either U–E or D–E orientation, in a single chain in the Na–Ba-phase both orientations (U,D)-E are realized simultaneously (Fig. 5a and b). In $Na_2Ca_6[SiO_4]_2[Si_2O_7]$ and $Na_2Mg_6[VO_4]_2[V_2O_7]$ a four layer stacking …ABCDABCD… is observed. The sequence of relative shifts is $\ldots+\delta,+\delta,-\delta,-\delta$

$+\delta,+\delta\ldots$ (see Fig. 4c and d). In the Na–Mg-vanadate, the kröhnkite-type chains occur in two different geometrical isomers (Fig. 5c). In one of the forms the tetrahedra are disordered among two positions (indicated by the letter S for "statistically disordered"). $Na_2Ca_6[SiO_4]_2[Si_2O_7]$ in turn can be derived from the Na–Mg-compound by an ordering process of the tetrahedra combined with additional rotational distortions. As examples, two of different chains are given Fig. 5d.

6. Conclusion

We would like to point out, that the results of our investigation corroborate the findings of Ohsato et al. [8] concerning the existence of a $K_2Ca_6Si_4O_{15}$ phase, i.e. the ternary phase diagram K_2O–CaO–SiO_2 given by Morey et al. [1,2] has to be modified. Furthermore, the partial melting of the pellet aimed at producing K_2CaSiO_4 by solid state reactions at 1000 °C, cannot be understood if the claimed melting point of 1600 °C reported by Morey et al. [1] for a sample with this composition is correct. Both observations clearly demonstrate that even chemically simple systems of main group element oxides are not as well understood, as one should expect. Still a lot of open problems concerning the phase relationships remain to be solved.

Acknowledgment

The authors would like to thank Bernhard Sartory for help with the chemical analysis using the electron microprobe.

Appendix A. Supporting Information

Supplementary data associated with this article can be found in the online version at doi:10.1016/j.jssc.2009.09.013.

References

[1] G.W. Morey, F.C. Kracek, N.L. Bowen, J. Soc. Glass Technol. 14 (1930) 149–187.
[2] G.W. Morey, F.C. Kracek, N.L. Bowen, J. Soc. Glass Technol. 15 (1931) 57–58.
[3] R.P. Gunawardane, F.P. Glasser, Z. Anorg. Allg. Chem. 411 (1975) 163–171.
[4] A.S. Berezhnoi, N.V. Lapina, E.V. Lifshits, E.P. Shevyakova, Neorg. Mater. 12 (1976) 1653–1658.
[5] H. Suzukawa, Zem. Kalk Gips 9 (1956) 390–396.
[6] N.F. Fedorov, E.R. Brodkina, Neorg. Mater. 2 (1966) 745–748.
[7] T. Akiyama, Y. Yao, S. Matsuno, Jpn. J. Soil Sci. Plant Nutr. 72 (2001) 484–488.
[8] H. Ohsato, T. Sugimura, S. Hayashi, T. Ogihara, Bull. Nagoya Inst. Technol. (1981) 123–130.
[9] V. Kahlenberg, R. Kaindl, D.M. Többens, J. Solid State Chem. 179 (2006) 1948–1956.
[10] E. Arroyabe, R. Kaindl, V. Kahlenberg, Z. Anorg. Allg. Chem. 635 (2009) 337–345.
[11] H. Hughes, Trans. Br. Ceram. Soc. 65 (1966) 661–679.
[12] P. Thy, B.M. Jenkins, C.E. Lesher, Energ. Fuel 13 (1999) 839–850.
[13] B. Olanders, B.M. Steenari, Biomass Bioenergy 8 (1995) 105–115.
[14] Y. Yasuko, A. Takashi, Jpn. J. Soil Sci. Plant Nutr. 72 (2001) 775–779.
[15] C. Vitale-Brovarone, E. Verné, J. Mater. Sci. Mater. Med. 16 (2005) 863–871.
[16] STOE & Cie GmbH, X-Area Version 1.39, Darmstadt, Germany, 2005.
[17] V. Kahlenberg, T. Messner, J. Appl. Crystallogr. 34 (2001) 405.
[18] V. Kahlenberg, Acta Crystallogr. B 55 (2001) 745–751.
[19] M.C. Burla, R. Caliandro, M. Camalli, B. Carrozzini, G.L. Cascarano, L. De Caro, C. Giacovazzo, G. Polidori, R. Spagna, J. Appl. Crystallogr. 38 (2005) 381–388.
[20] R.H. Blessing, Acta Crystallogr. A 51 (1995) 33–38.
[21] G.M. Sheldrick, SHELX97-Programs for Crystal Structure Analysis (Release 97-2), University of Göttingen, Germany, 1998.
[22] E. Dowty, ATOMS Version 5.1, Shape Software, 2000.
[23] F. Liebau, Structural Chemistry of Silicates—Structure, Bonding and Classification, Springer Verlag, Berlin, Heidelberg, New York, Tokyo, 1985.
[24] R. Robinson, G.V. Gibbs, P.H. Ribbe, Science 172 (1971) 567–570.
[25] A.J.C. Wilson (Ed.), International Tables for Crystallography, Vol. C, Kluwer Academic Publishers, Dordrecht, The Netherlands, 1995.
[26] S.E. Wright, J.A. Foley, J.M. Hughes, Am. Mineral. 85 (2000) 524–531.
[27] U. Kolitsch, M. Fleck, Eur. J. Mineral. 18 (2006) 471–482.
[28] F.C. Hawthorne, Acta Crystallogr. A 39 (1983) 724–736.
[29] S.V. Krivovichev, P.C. Bruns, Solid State Sci. 5 (2003) 481–485.
[30] R. Dovesi, V.R. Saunders, C. Roetti, R. Orlando, C.M. Zicovich-Wilson, F. Pascale, B. Civalleri, K. Doll, N.M. Harrison, I.J. Bush, Ph. D'Arco, M. Llunell, CRYSTAL06—User's Manual, University of Torino, Torino, 2006.
[31] C.M. Zicovich-Wilson, F.J. Torres, F. Pascale, L. Valenzano, R. Orlando, R. Dovesi, J. Comput. Chem. 29 (13) (2008) 2268–2278.
[32] R. Dovesi, C. Roetti, C. Freyria Fava, M. Prencipe, V.R. Saunders, Chem. Phys. 156 (1991) 11–19.
[33] P.A.M. Dirac, Proc. Cambridge Philos. Soc. 26 (1930) 376.
[34] S.H. Vosko, L. Wilk, M. Nusair, Can. J. Phys. 58 (1980) 1200.
[35] D.D. Johnson, Phys. Rev. B 38 (1988) 12807–12813.
[36] K.F. Hesse, G. Stümpel, Z. Kristallogr. 177 (1986) 143–148.
[37] R.A. Howie, V.V. Ilyukhin, Nature 269 (1977) 231.
[38] T. Armbruster, F. Röthlisberger, Am. Mineral. 75 (1990) 963–969.
[39] R.A. Tamazyan, A. Malinovskii, M.J. Sirota, Sov. Phys. Crystallogr. 32 (1987) 519–522.
[40] A. Mitiaev, A. Mirinov, R. Shpanchenko, E. Antipov, Acta Crystallogr. C 60 (2004) i56–i58.
[41] A.M. Il'inets, V.V. Iliukhin, N.V. Belov, N.N. Nevskii, Dokl. Akad. Nauk SSSR 267 (1982) 1125–1127.
[42] M. Wierzbicka-Wieczorek, Ph.D. thesis, University of Vienna, 2007.